Korean J. Chem. Eng., 37(11), 2041-2053 (2020)
DOI: 10.1007/s11814-020-0657-4

pISSN: 0256-1115
eISSN: 1975-7220

A novel CFD simulation of H_2 separation by Pd-based helical and straight membrane tubes

Hamid Abdi*,†, Nader Pourmahmoud*, and Jafar Soltan**

*Mechanical Engineering Department, Urmia University, Urmia, Iran
**Chemical Engineering Department of Chemical and Biological Engineering, University of Saskatchewan, Saskatoon, SK, S7N 5A9, Canada
(*Received 8 May 2020 • Revised 8 July 2020 • Accepted 5 August 2020*)

Abstract−A novel three-dimensional CFD simulation of H_2 gas permeation through dense palladium (Pd) membrane was developed. Due to discontinuity of flow in a membrane, usually, gas diffusion process is simulated by introducing source and sink terms. In a novel approach, an analogy between heat and mass transfer is considered. The most important advantage of this approach is that there is no need to define sink and source terms, and the membrane thickness is considered as a solution domain without separating the geometry adjacent to the membrane. Also, it allows the modeling of multilayer membranes with different mechanisms of diffusion, separately. The effect of membrane geometry on the hydrogen separation was investigated using the straight and helical modules by defining user-defined function (UDF) and user-defined scalars (UDS). The results showed an average flux and H_2 recovery enhancement of 20% and 13% for helical configuration, respectively. The influence of the feed gas and sweep gas flow rates, helix pitch, coil diameter, pressure difference, and module temperature on hydrogen separation was also investigated. The proposed simulation model was validated using the experimental data. The results indicated that this method has a maximum error of about 10% for H_2 flux.

Keywords: Numerical Simulation, Palladium (Pd) Membrane, Straight and Helical Tubes, H_2 Separation

INTRODUCTION

Hydrogen, the most occurring component taking up 75% of the universe, plays a great role as an energy carrier. Reduced emissions of pollutants and greenhouse gases when oxidized as fuel, different storage forms (unlike electricity), different ways of transportation, and capability to being produced from multiple sources like fossil fuels, uranium, and renewable energy sources make H_2 an ideal energy carrier [1,2]. Unfortunately, because there is no free hydrogen in nature and it is in combination with other elements, it must be extracted from other materials, such as hydrocarbons, water, and biomass [3]. Hydrocarbons (natural gas (NG) and petroleum) account for 78% of the world's hydrogen production. About 4% of hydrogen is produced by water electrolysis and about 18% is produced from coal [4]. There are several hydrogen production methods such as thermochemical, electrochemical, photobiological, and photochemical [5]. The most commonly used thermochemical method in hydrogen production is steam reforming (SR) of methane [6]. In addition to steam reforming (SR) of methane, one of the potential methods for clean hydrogen production in special conditions is the catalytic decomposition of ammonia. In this reaction, nitrogen is produced without any CO or CO_2 as by-product [7-9]. In these methods, hydrogen-rich gas rather than pure hydrogen is obtained, and for some applications like proton-exchange membrane (PEM) fuel cells, pure hydrogen is needed, so separation and purification of hydrogen are crucial [10]. The membrane separation method is one of the best methods of purification due to quieter performance without moving parts, lower cost to manufacture, lower energy consumption, continuous separation and higher hydrogen selectivity [11-14]. Dense metallic based membranes, especially Palladium (Pd) membranes, have received much attention due to the ability of hydrogen permeation in a dissociative form with a theoretically infinite selectivity [15,16]. Because pure palladium under operating conditions cannot operate for a long lifetime, it should be alloyed with other metals, like aluminum, copper, and indium [16]. There are different methods for studying the behavior of membranes, e.g., simulation methods or experimental approaches. Because obtaining data like concentration or pressure on the inner flow structures of a module is difficult and expensive in the experimental method, the simulation approach is preferred by some researchers [17-21]. The simulation approach is not only cheaper and easier but also provides data for the whole geometry [22-27]. Computational fluid dynamic (CFD) modeling as a simulation approach has many advantages over the experimental method. It provides a good insight into the gas separation processes through detailed temporal and spatial data [28-30]. In the CFD method by varying different parameters of the membrane system, performance can be investigated; thus, it can greatly reduce the cost related to experimental work, but for validation of these models it should be combined with experimental method. Takaba et al. [31] numerically investigated concentration polarization in H_2/CO separation membranes. Abdel-Jawad et al. [32] used CFD to investigate diffu-

†To whom correspondence should be addressed.
E-mail: hm.abdi@urmia.ac.ir

sion through inorganic molecular sieve silica (MSS) membranes. They solved the problem by coupling the Navier-Stokes equations and Stefan-Maxwell gas-through-gas diffusion model and the phenomenological equation that is exclusively used on the membrane. They showed that the diffusion through the membrane occurs much slower than gas-through-gas on the feed and permeate domain. Wei-Hsin Chen et al. [13] studied the permeation of hydrogen and concentration polarization in dense palladium (Pd) membrane tube. They used a numerical method introducing a source-sink pair obeying Sieverts' law in the membrane. The results showed that counter-current flow has better hydrogen separation compared to the co-current one, and the increasing flow rates of feed gas and sweep gas can efficiently affect the H_2 permeation by increasing the concentration polarization. Coroneo et al. [33] simulated inorganic membrane modules for gas mixture separation using a computational fluid dynamic (CFD) approach. They introduced source and sink terms at the membrane boundary cells. They used a CFD approach in three kinds of membranes, and results showed a good agreement with experimental data. Chen et al. [34] investigated the influence of geometry and flow patterns on hydrogen separation in a Pd-based membrane tube. The effects of Reynolds numbers, shell size, baffle, and pressure difference on hydrogen mass transfer across the membrane were evaluated. Ben-Mansour [35] conducted a study on the effect of different parameters like the permeate outlet pressure, the mass flow rate of mixed feeding and sweeping gases and membrane length on the total mass flow rate, the mass fraction of CO_2 and the mass flow rate of CO_2 in the permeate outlet. Their results revealed that using sweep gas has a significant impact on the increasing mass flow rate of CO_2 in the permeate side, and the increasing membrane length increases the mass fraction and mass flow rate of CO_2 in permeate outlet. Ghohe et al. [36] numerically investigated H_2 separation by a conical palladium membrane. They used the solution-diffusion mechanism of mass transfer in the palladium membrane and studied four different flow patterns. Their results showed that the conical membrane module with an upper diameter of 2 mm and a bottom diameter of 16 mm has the highest average flux across the other studied cases. Among four different flow patterns, the counter-current flow pattern has the highest flux for the case in which the cross-section is reduced along with the length of the membrane. In all the papers mentioned, because of the discontinuity of gas flow in the membrane it is not possible to use the Navier-Stoke equations, and this problem is solved by means of source terms. In this method, the membrane is assumed as a zero-thickness wall. In the feed and permeate sides, the first rows of the mesh cells are considered sources. This means that gas disappears from the feed zone and emerges at the permeate zone. Although this model is a useful method for simulating the process of separating gases with membranes, it can, however, have errors. In reality, the process of gas absorption by the membrane is done on the feed zone and disposed of it, is done on the permeate zone at the boundary of membrane and fluid. So, for introducing the source and sink terms, it requires a user defined function (UDF) on the adjacent membrane mesh cells instead of the membrane boundary, and this is not compatible with the actual physics of the problem. In the present study, a new method for CFD modeling has been developed for the process of gas separation using membranes, which is more compatible with the physics governing the problem. There is no need to define sink and source terms, and the membrane thickness is considered as a solution domain without separating the geometry adjacent to the membrane. Also, it allows the modeling of multilayer membranes with different mechanisms of diffusion, separately. The objective of the present study was to simulate the H_2/N_2 gaseous mixture separation numerically in Pd-based hollow fiber membranes with different geometries and different feed gas flow rates by using new CFD model. The results were validated with the experimental data and were in good agreement, which indicates the validity of the suggested method.

MODEL DEVELOPMENT

As mentioned, the main problem with modeling the gas separation processes with membranes is that the flow behavior in the membrane pores and cavities cannot be predicted using Navier-Stokes equations. Hence, it is necessary to use semiconducting relationships to predict the flow rate of the membrane, regardless of the details and how the fluid moves in the membrane pores. In the previous section, a commonly used sink-source method was mentioned that is used by many to model the membrane. In this study, a new method for CFD modeling of membrane separation is suggested. For this purpose, the similarities between the heat transfer and mass transfer, and then the basis of this method based on these similarities, are discussed.

1. Similarities between Mass Transfer and Heat Transfer

Comparing the relations and mechanisms governing the two phenomena of mass and heat transfer showed that mass transfer in many respects is comparable to heat transfer and the relations of heat transfer and mass transfer are very similar [37]. There are three mechanisms of heat transfer: conduction, convection, and radiation; also mass is transferred by conduction (diffusion) and convection only. The rate of heat conduction is expressed by Fourier's law of heat conduction as:

$$\dot{Q}_{cond} = -KA\frac{dT}{dx} \tag{1}$$

where K ($W \cdot m^{-1} \cdot k^{-1}$) is the medium conductivity, and A (m^2) is the area normal to the heat transfer direction.

The rate of mass diffusion of a chemical species *i* is expressed by Fick's law of diffusion as:

$$J_{diff} = -D_{ij}A\frac{dC_i}{dx} \tag{2}$$

where D_{ij} ($m^2 \cdot s^{-1}$) is the species diffusion coefficient in the mixture, and C_i ($mol \cdot m^{-3}$) is the concentration of the species *i* in the mixture.

The heat convection rate is expressed by Newton's law of cooling as:

$$\dot{Q}_{conv} = h_{conv}A_s(T_s - T_\infty) \tag{3}$$

where h_{conv} ($w \cdot m^{-2} \cdot K^{-1}$) is the heat transfer coefficient, A_s (m^2) is the surface area, T_s (K) is the surface temperature, and T_∞ (K) is the fluid temperature.

The rate of mass convection is expressed as:

$$J_{conv} = h_{mass} A_s (C_s - C_\infty) \quad (4)$$

where h_{mass} ($m \cdot s^{-1}$) is the mass transfer coefficient, A_s (m^2) is the surface area, $C_s - C_\infty$ is the concentration difference across the concentration boundary layer.

2. New CFD Method

In the previous section, the similarities between heat and mass transfer were described. For both heat conduction and mass diffusion, it can be observed that the differential equations are of the same form; therefore, the diffusion of the species in the mixture of gas through the membrane can be considered to be the same as the thermal conduction in the solid object. A diffusion coefficient of membrane, like the conductivity coefficient, can be considered as a property of the membrane, which is a relation based on the mechanisms of diffusion through the membrane and the experimental coefficients. In fact, in this method the concentration of species in the mixture (feed and permeate side) is achieved by applying the species conservation equation. In the membrane, like the heat transfer, only diffusive term of the species conservation equation is used. Therefore, species in the mixture are transferred from the feed side through the membrane as a nonporous solid to the permeate side by conduction (diffusion). Thus, the process of transferring of species is simulated through the membrane. The diffusion equation in the membrane is expressed as:

$$\nabla(-D_{im} \nabla C_i) = 0 \quad (5)$$

where D_{im} is the species *i* diffusion coefficient in the mixture, which is either empirically obtained in the laboratory for any type of membrane as an intrinsic property or obtained through the diffusion mechanisms governing the membrane.

2-1. The Diffusion Coefficient in the Membrane

Due to the structure and morphology of the membrane, as well as its shape and size and other characteristics, the gas components can pass through membranes by different transfer mechanisms. The membrane used in this study is pd/α-Al_2O_3. In this type of membrane, the solution diffusion mechanism is dominant. The gas molecules on one side of the membrane are absorbed, dissolve in the membrane material, pass through the membrane, and desorb on the other side [38]. This mechanism follows Sievert's law which is expressed as [39]:

$$J_{sievert} = Q_0 \exp\left(-\frac{E_a}{RT}\right)(dP_i)^n \quad (6)$$

where Q_0 ($mol \cdot m^{-2} \cdot s^{-1} \cdot pa^{-n}$) is the pre-exponential factor, E_a ($kJ \cdot mol^{-1}$) is activation energy and ΔP_i (pa) is partial pressure difference of species i in the membrane and R is universal gas constant ($J \cdot K^{-1} \cdot mol^{-1}$) and T is temperature (k). The exponent n is determined experimentally, which varies from n=0.5 to n=1. The value of n reflects the dominant mechanism of gas transport through the Pd membrane. When n=0.5, it means that the bulk diffusion is dominant in transport, 0.5<n<1 indicates that both surface process (adsorption on and desorption from the membrane surface) and bulk diffusion control the transport and when surface process dominates, the exponent is equal to n=1. According to the ideal gas equation:

$$C_i = \frac{P_i}{RT} \quad (7)$$

Therefore, by replacing the concentration with the pressure from the above equation, Eq. (6) can also be written based on the concentration of the mixed species.

$$J_{sievert} = Q_0 (RT)^n \exp\left(-\frac{E_a}{RT}\right)(dC_i)^n \quad (8)$$

As mentioned, only a diffusive term of the species conservation equation is used in the membrane, and this equation is expressed as:

$$J_{diff} = -D_{ij} \frac{dC_i}{dx} \quad (9)$$

By comparing Eq. (8) with Eq. (9) the diffusion coefficient is obtained.

$$D_{ij,\,sievert} = Q_0 \delta (RT)^n \exp\left(-\frac{E_a}{RT}\right)/(\Delta C_i)^{1-n} \quad (10)$$

Where δ (m) is the membrane thickness. For a Pd/α-Al_2O_3 membrane used in this study, $Q_0 = 3.12 \times 10^{-5}$ ($mol \cdot m^{-2} \cdot s^{-1} \cdot pa^{-1}$) E_a = 13.9 ($KJ \cdot mol^{-1}$) and the exponent is equal to n=1 [40].

2-2. Boundary Conditions at the Boundaries of Fluid with Membrane

Similar to the heat transfer at the boundaries of the membrane with fluid, a conjugate boundary condition is used. This boundary condition indicates the equivalence of mass diffusion rate on both sides of the boundary (fluid and solid).

$$-D_{ij} \frac{dC_i}{dx} = h_{mass}(C_{i,s} - C_{i,\infty}) \quad (11)$$

Thus, by applying this boundary condition to the boundaries of the membrane with the fluid on the feed and permeate sides, the process of absorbing and disposing of the species by the membrane is also fully compatible with the actual physics of the problem, and there is no need to separate the geometry adjacent the membrane to define sink and source terms.

3. Governing Equations

Fig. 1 shows a schematic diagram of the membrane tube and straight and helical geometries in this study. Feed gas flow enters from the inlet; a gas species in the feed domain permeates to the permeate domain through the membrane. The remaining part of the feed gas exits as retentate, and the separated gas in the permeate domain flows to the outlet. The tube length for both helical and straight geometries is 100 mm, and the diameter of shell and tube is 6.25 mm, and 5 mm, respectively, and the membrane thickness is 250 μm.

The flow in feed and permeate domain is continuous and the governing equations in these domains are the same. Where the ideal gas equation and continuity, momentum, and species conservation equations are as below:

Continuity equation:

$$\nabla \cdot \rho \vec{V} = 0 \quad (12)$$

where ρ is fluid density ($kg \cdot m^{-3}$) and v is velocity ($m \cdot s^{-1}$).

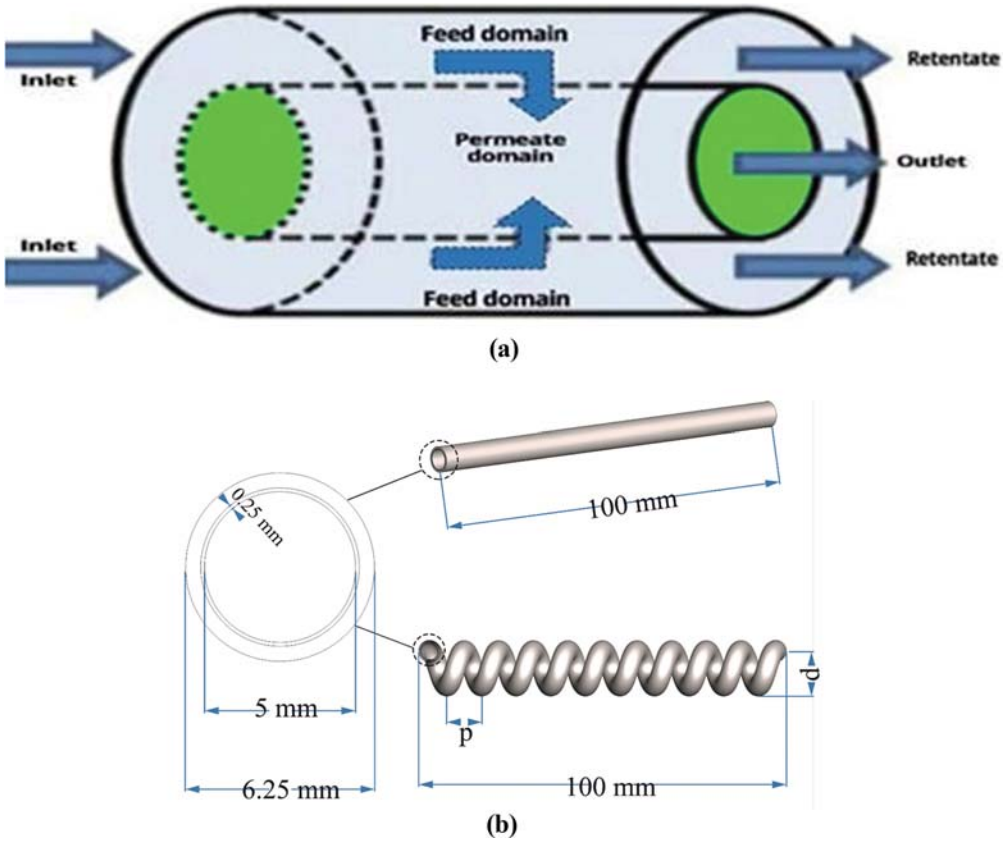

Fig. 1. Schematics of (a) permeation system (b) straight and helical geometries.

Table 1. Boundary conditions of different domains

Domain	Boundary	Momentum	Species
Feed	Inlet	$v_x=Q/A$	$C_i=x_iC_{tot}$
	Outlet	$p=p_{total}$	$\nabla C_i=0$
	Shell	$v_x=v_y=v_z=0$	$\nabla C_i=0$
Membrane	Shell	$v_x=v_y=v_z=0$	$D_{ij,m}\left.\frac{dC_i}{dx}\right\|_{mem}=D_{ij,F}\left.\frac{dC_i}{dx}\right\|_{feed}$
	Tube	$v_x=v_y=v_z=0$	$D_{ij,m}\left.\frac{dC_i}{dx}\right\|_{mem}=D_{ij,p}\left.\frac{dC_i}{dx}\right\|_{permeate}$
Permeate	Outlet	$p=p_{total}$	$\nabla C_i=0$
	Wall	$v_x=v_y=v_z=0$	$\nabla C_i=0$

Momentum equation:

$$\nabla\cdot\rho\vec{V}\vec{V}=-\nabla P+\mu\nabla^2V \quad (13)$$

Here p is pressure (Pa), and μ is viscosity (Pa·s).

Species equation:

$$\nabla\cdot C_i\vec{V}=\nabla(-D_{ij}\nabla C_i) \quad (14)$$

where C_i is the mole fraction of species *i* and D_{ij} is diffusion coefficient ($m^2\cdot s^{-1}$).

Equation of state:

$$P_i=C_iRT \quad (15)$$

where R is the universal gas constant ($J\cdot K^{-1}\cdot mol^{-1}$), and T is the temperature (k).

4. Boundary Conditions

The separation system consists of three domains: feed, membrane and permeate. The types of boundaries on these domains are listed in Table 1.

5. Properties of the Gas Mixture

The properties of gas mixture such as density, viscosity and diffusion coefficient are expressed as follows.

5-1. Density

The mixture is assumed to be an ideal gas; therefore, the density of the mixture can be calculated from the ideal gas equation.

$$\rho_{mix} = \frac{P_{mix}}{\left(\frac{R}{M_{mix}}\right)T} \tag{16}$$

where ρ_{mix} (kg·m^{-3}) is mixture density, Pmix (pa) is mixture pressure and M_{mix} is mixture molar mass (g mol^{-1}).

5-2. Viscosity

The viscosity of the mixture is calculated by Herning and Zipperer correlation as:

$$\mu_{mix} = \frac{\Sigma x_i \sqrt{M_i}\mu_i}{\Sigma x_i \sqrt{M_i}} \tag{17}$$

where μ_{mix} (pa·s) is the mixture viscosity, μ_i is species *i* viscosity, x_i is a molar fraction of species *i* and M_i (g mol^{-1}) is species *i* molar mass.

5-3. Diffusion Coefficient

If the diffusion coefficient is known at a specified temperature and pressure, then at different temperatures and pressures it can be determined by [37]:

$$\frac{D_{ij,1}}{D_{ij,2}} = \frac{P_2}{P_1}\left(\frac{T_1}{T_2}\right)^{\frac{3}{2}} \tag{18}$$

According to the above equations, the gas mixture properties are not constant and are functions of components concentration, temperature, and pressure. Therefore, they must be calculated by user-defined function (UDF). For hydrogen, nitrogen, and steam, physical properties such as viscosity and diffusion coefficient at a pres-

Table 2. A list of properties of three gases at different temperatures and 1 bar

Properties	T=300 °C	T=350 °C	T=400 °C	T=500 °C	T=600 °C	T=700 °C
H_2 viscosity (pa·s)	1.4×10^{-5}	1.48×10^{-5}	1.57×10^{-5}	1.73×10^{-5}	1.88×10^{-5}	2×10^{-5}
H_2 viscosity (pa·s)	2.85×10^{-5}	3×10^{-5}	3.16×10^{-5}	3.45×10^{-5}	3.7×10^{-5}	3.95×10^{-5}
H_2O viscosity (pa·s)	2×10^{-5}	2.23×10^{-5}	2.45×10^{-5}	2.85×10^{-5}	3.24×10^{-5}	3.64×10^{-5}
H_2 diffusion coefficient ($m^2\cdot s^{-1}$)	23.81×10^{-5}	26.19×10^{-5}	30.31×10^{-5}	37.31×10^{-5}	44.78×10^{-5}	52.69×10^{-5}

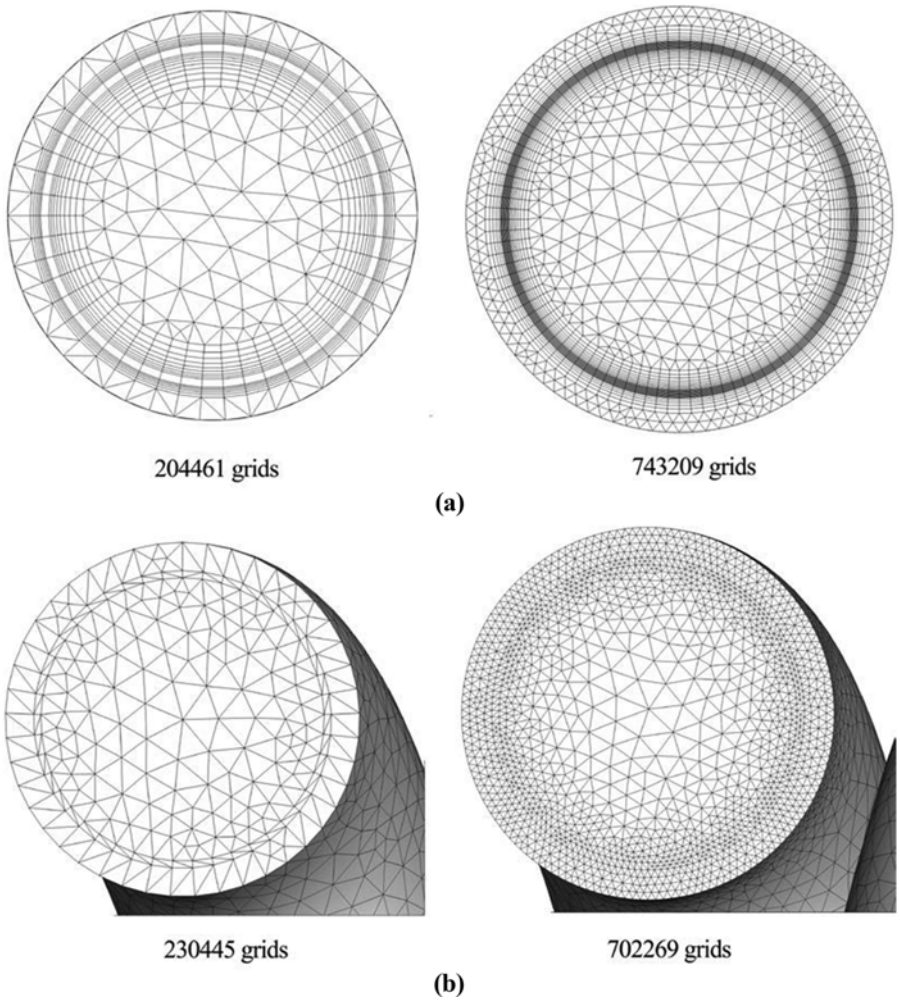

Fig. 2. Schematics of (a) straight and (b) helical computational domains.

sure of 1bar and two temperatures of 350 °C and 500 °C are listed in Table 2 [37].

5-4. H_2 Recovery

It is the percentage of H_2 that permeates through the membrane, and it represents the efficiency of the separation system.

$$H_{2\ recovery} = \left(1 - \frac{C_{H_2,\ retentate}}{C_{H_2,\ feed}}\right) \times 100 \quad (19)$$

6. Numerical Method

The commercial software ANSYS Fluent® 19.0 was used to solve the governing equations. As mentioned, the equations include Navier-Stokes, continuity, and species equations. The momentum and continuity equations are applied according to Fluent default, but for species equation, user-defined scalars (UDS) was used. For pressure-velocity coupling, the semi-implicit method for pressure linked equations (SIMPLE) scheme, and for spatial discretization, the second-order upwind scheme were used. The feed gas mixture consists of 50% of N_2 and 50% of H_2; flow regime in both feed and permeate sides was laminar. The separation process was carried out under constant temperature and steady conditions; flow concentration in both feed and permeate sides was constant. Permeability of membrane was infinite for H_2, and zero for other species. Volume forces were neglected, and the gas mixture was considered as an ideal gas in all domains. Mesh independency for both straight and helical geometries was studied. As shown in Fig. 2, both tetrahedron and hexahedron meshes were used for straight tube and for the helical tube. Only tetrahedron meshes were used in the membrane domain due to the small thickness of the membrane. According to Fig. 3 for straight tube, the number of appropriate meshes was about 743209, and for helical tube about 702269.

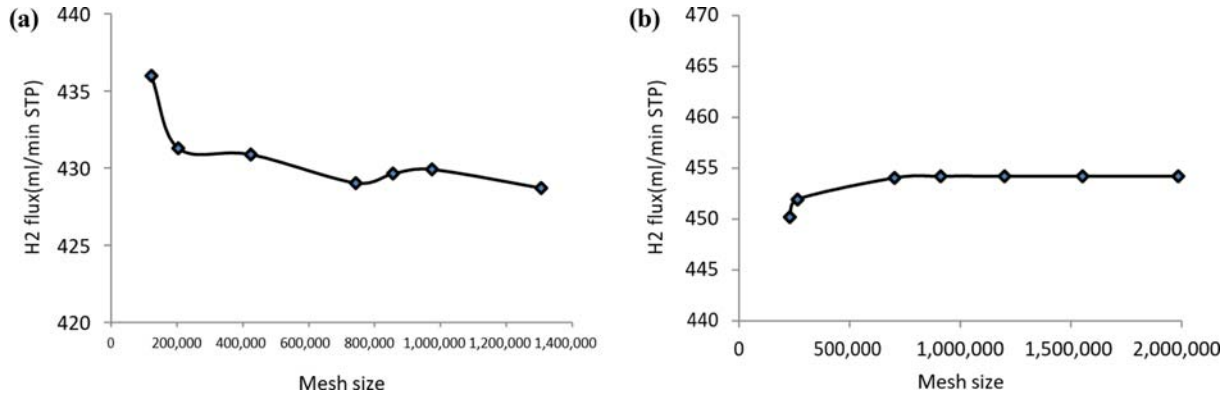

Fig. 3. Mesh independency of (a) straight tube (b) helical tube.

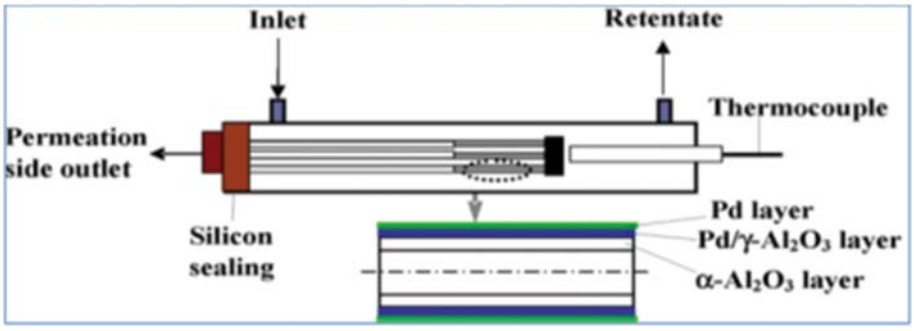

Fig. 4. Schematics of membrane module used in the study of Wang et al.

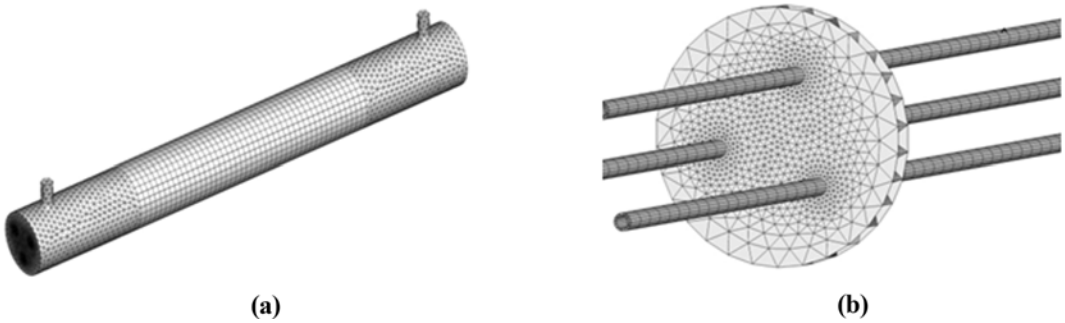

Fig. 5. Schematics of (a) computational grid used in this study (b) Interior cutting of module.

MODEL VALIDATION

The proposed model was evaluated using experimental data from Wang et al. [40] to determine the validity and accuracy of the model. The membrane used in by Wang et al. was thin Pd/α-Al_2O_3 HF membrane, which has been used to separate H_2 from an H_2N_2 gas mixture. Fig. 4 illustrates the membrane module used by Wang et al., which contains three hollow fiber membranes of 4.5 cm length inserted into tubes of 10 cm diameter. Because sweep gas was not used in their experiments, one end of the membranes was blocked and the other end was considered to be the output of the permeate side. Three-dimensional meshed geometry of membrane is shown in Fig. 5. Due to the asymmetric geometry, and also to achieve smaller meshes in the vicinity of membranes with a high concentration gradient, a tetrahedron mesh was used. The total number of meshes used to gain independence from the mesh was 192,847. Also, the molar concentration of hydrogen is shown in different areas of the module in Fig. 6. As can be seen, the molar concentration of hydrogen gradually decreases from entry (left) to exit (right). In fact, this indicates concentration polarization in the axial direction. Fig. 7 shows the results of the new numerical model in comparison to experimental data of Wang et al. [40] for the separation of H_2N_2 mixture at temperatures of 350 °C and 500 °C. Model predictions show very good agreement with the experimental data. The maximum mean absolute error is 10% for both the mixtures of 350° and 500 °C, and the error average values are 9% and 7%, respectively for mixtures of 350° and 500 °C.

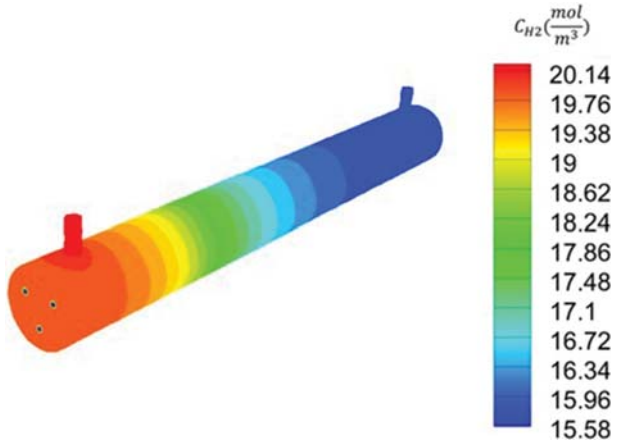

Fig. 6. H_2 concentration contours for the feed flow of 160 ml/min at 500 °C.

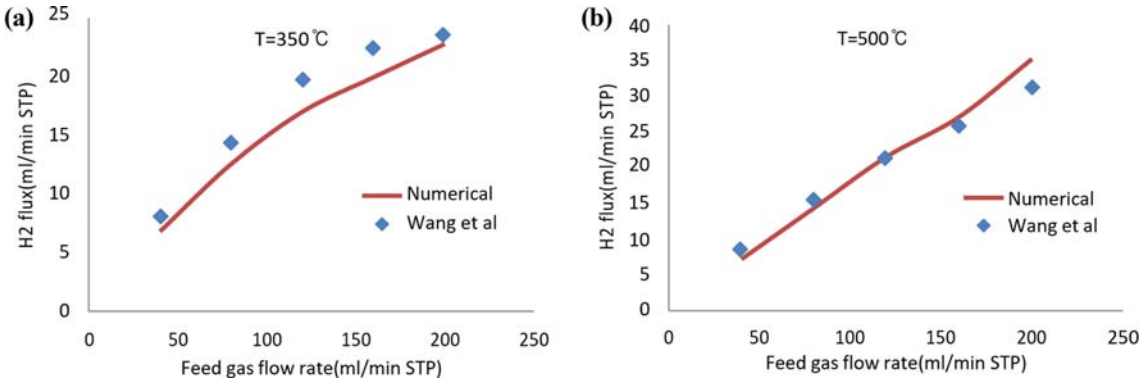

Fig. 7. Flow rate of H_2 at the outlet of the permeate domain vs. different flow rates of feed gas at (a) 350 °C and (b) 500 °C.

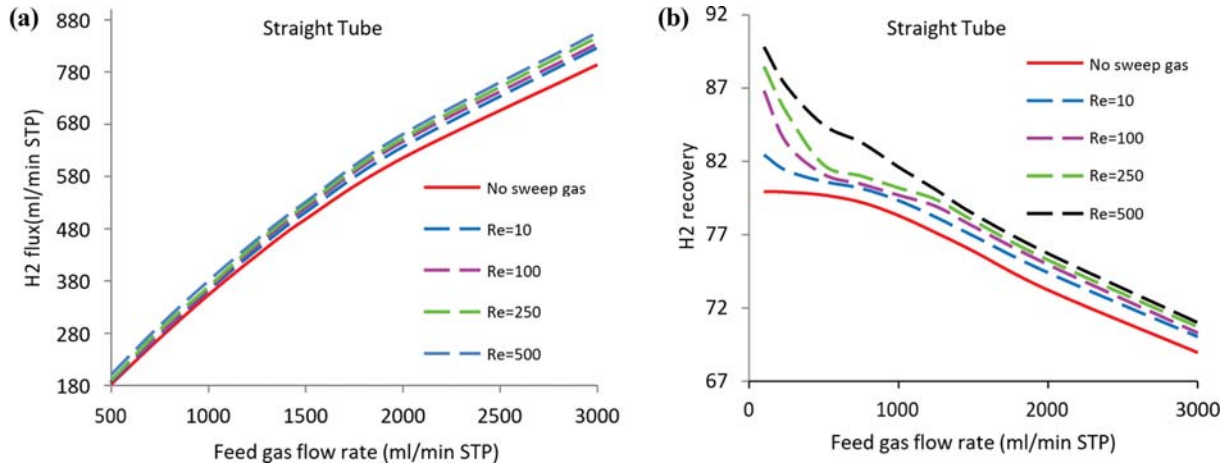

Fig. 8. Distribution of (a) H_2 flow rate at the outlet of the permeate domain and (b) H_2 recovery in the straight tube for the different flow rates of feed gas in different Reynolds number of sweep gas.

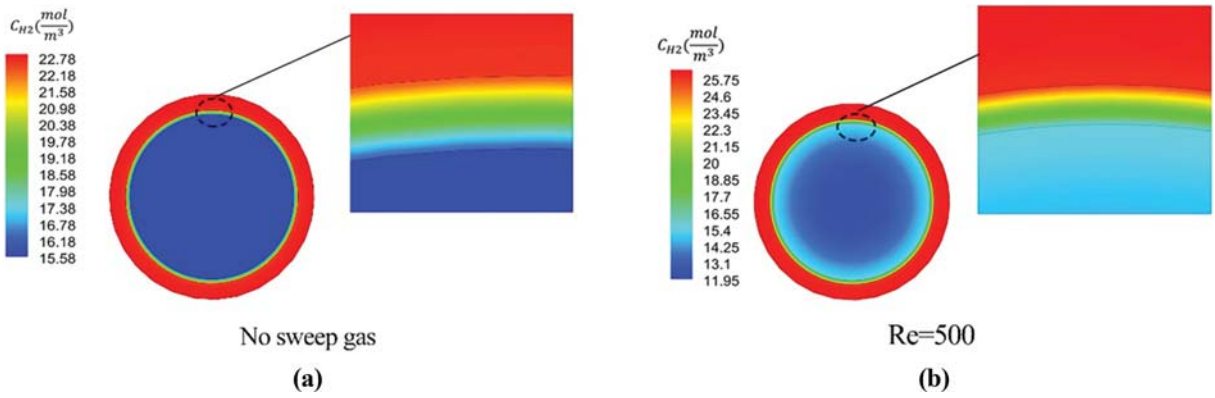

Fig. 9. H_2 concentration contours for the feed flow rate of 1,250 ml/min of (a) straight tube without sweep gas and (b) with sweep gas Re=500.

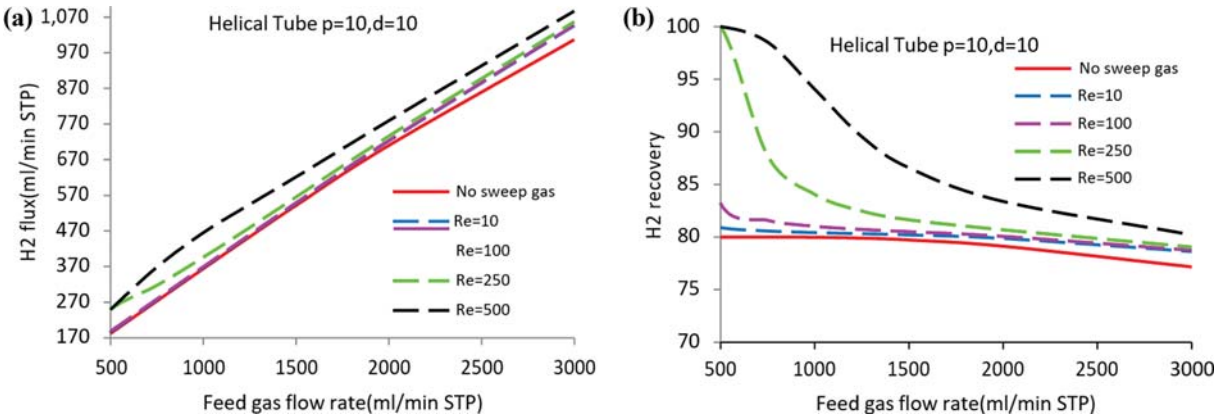

Fig. 10. Distribution of (a) H_2 flow rate at the outlet of the permeate domain and (b) H_2 recovery in the helical tube for the different flow rates of feed gas in different Reynolds number of sweep gas.

RESULTS AND DISCUSSION

1. Effect of Feed Gas and Sweep Gas Flow Rate

Fig. 8(a) shows the effect of feed flow rate and also sweep gas counter-current flow rate on the hydrogen separation at 500 °C. As expected, the amount of permeation will increase proportionately with increasing feed gas flow, but, as can be seen, the rate of increase in permeation rate decreases. It is also observed that the use of sweep gas flow increases the permeation rate, and this increase in permeation rate increases with increasing feed flow because at lower flow rates, almost the entire hydrogen of the feed gas has the opportunity to pass through the membrane that is shown in Fig. 8(a). H_2 recovery for different flow rates of feed gas and for different Reynolds numbers of sweep gas is shown in Fig. 8(b). In Fig. 9, increase in the sweep gas Reynolds number leads to an increase of H_2 permeation by removing H_2 on the permeate side adjacent to the membrane and increasing the gradient of the partial concentration of H_2 across the membrane. Another point that is inferred is that for a specific value of feed gas flow rate, H_2 flux increase is not increasing proportionally to the rate of increase of sweep gas Reynolds number. For example, for feed gas flow of 3,000 (ml/min) with no sweep gas, H_2 flux is 793 (ml/min), and its value is 830 (ml/min) if the sweep gas with Reynolds number of 50 is used. That is an increase of about 4.6% in H_2 flux. However, if Reynolds number of sweep gas is doubled, H_2 flux reaches 833 (ml/min). That is about a 0.3% increase. Also, with increasing Reynolds number of sweep gas, the amount of pressure drop on the permeate side increases; therefore, it seems that using sweep gas with higher Reynolds number is not efficient due to higher energy consumption.

Fig. 10(a) and (b) show H_2 permeation flux and H_2 recovery for different levels of feed gas flow rates respectively for a helical geometry with a helix pitch of 10 mm and a coil diameter of 10 mm. It is observed that similar to the straight tube with increasing feed gas flow rate, the flux of H_2 at permeate side increases and H_2 recovery decreases. In addition, for the specific amount of feed gas flow rate by increasing the Reynolds number of sweep gas, H_2 flux, and H_2 recovery increase.

According to Fig. 11, compared to the straight tube, the helical tube gives a better efficiency of hydrogen separation. It is due to the higher value of surface-to-volume ratio and also the existence of secondary flows in the helical tube. When a fluid flows in a curved tube, the pressure difference between the internal and external walls of the tube causes a centrifugal force that forces the fluid to flow toward the outer wall; thus a secondary flow is created. In Fig. 11(a), for both membrane separation systems with and without sweep

gas, the helical tube has the best H_2 separation flux, and this difference is greater for large amounts of feed gas flow rate due to stronger centrifugal forces. For example, for 100 (ml/min) of feed gas flow with Re=500, H_2 flux of helical tube is about 14% higher than straight tube, and for 3,000 (ml/min) flow rate of the feed gas, this difference is about 27%. The average enhancement of H_2 separation flux for different values of feed gas flow with Re=500 is about 20%. In addition, it is obvious from Fig. 11(b) that the amount of recovered H_2 in helical tubes is higher than the straight one for all amounts of feed gas flow rate, and the average enhancement of recovered H_2 different values of feed gas flow with Re=500 is about 13%.

There are two important parameters in coiled configuration, the pitch of helix p and coil diameter d; the effect of these two parameters on the permeation rate of H_2 is illustrated in Fig. 12. It can be observed that by increasing the value of coil diameter, H_2

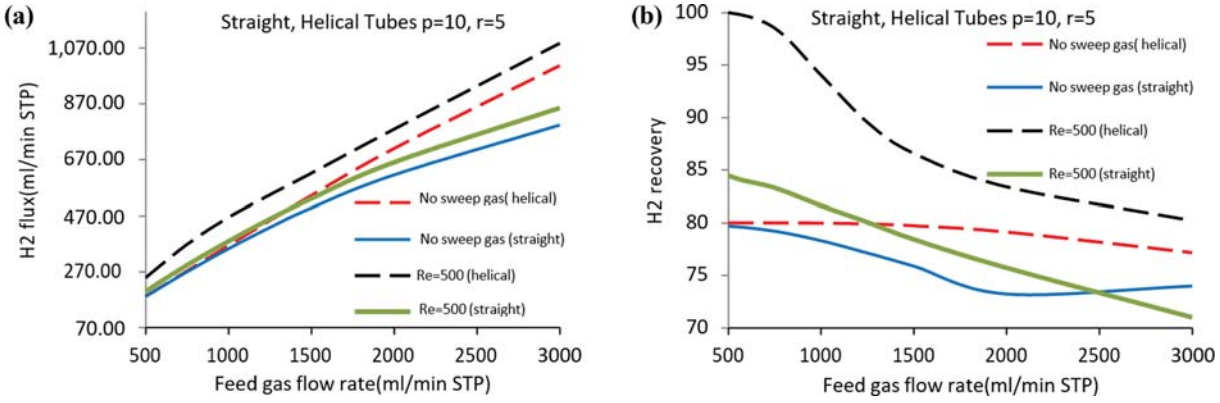

Fig. 11. Comparison of (a) Flow rate of H_2 at the outlet of the permeate domain and (b) H_2 recovery of the straight tube with helical one.

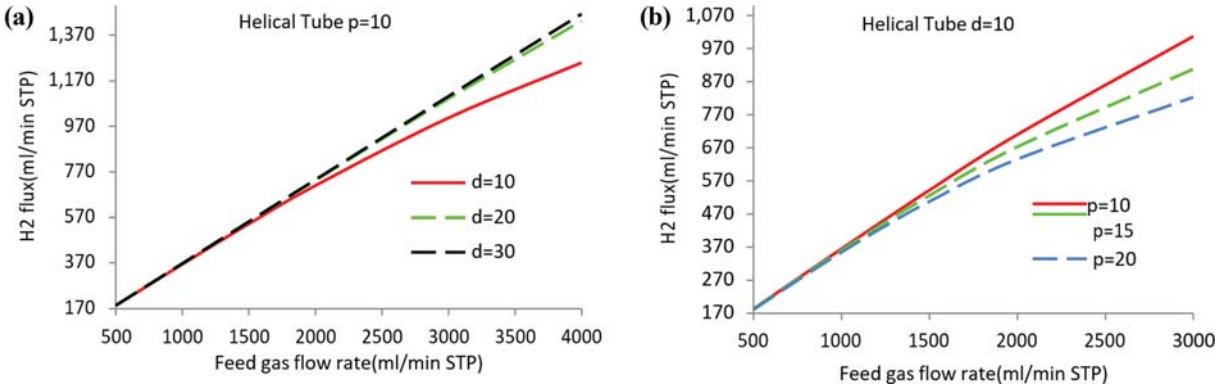

Fig. 12. Flow rate of H_2 at the outlet of the permeate domain of helical tube for different flow rates of feed gas in different (a) coil diameters and (b) helix pitches.

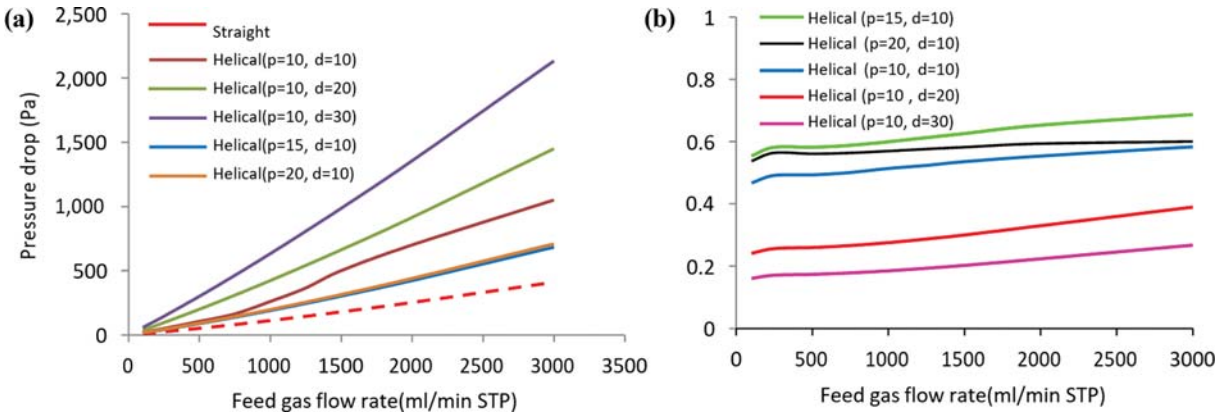

Fig. 13. (a) Comparison of pressure drop in straight and helical tubes and (b) comparison of overall performance criteria of helical tubes for different flow rates of feed gas.

permeation flux increased, and this increase is dominant at high values of feed gas flow rates. Also, it is shown that the rate of increase of H_2 permeation flux decreased by increasing coil diameter. The effect of coil pitch on H_2 permeation flux is presented in Fig. 12(b). By decreasing the value of the helix pitch due to the increasing value of the surface to volume ratio, H_2 permeation flux increased. By comparing Figs. 12(a), 12(b), it can be concluded that the effect of changes in helix pitch on the H_2 permeation flux is greater than changes in coil diameter. By investigating the Figs. 12(a), 12(b), it is seen that by decreasing the value of helix pitch for different amounts of feed gas flow for p=20 mm and p=10 mm H_2 permeation flux increased by an average of 6% but for d=10 mm and d=30 mm, that increased by an average of 2.2%.

Fig. 13(a) shows the effect of using different helical geometries on pressure drop for different values of feed gas flow. As can be seen, increasing the feed gas flow rate leads to a higher pressure drop between the inlet and outlet of tubes. Also, helical tubes have higher pressure drop than straight tube, and by increasing the value of coil diameter, pressure drop increased, and by increasing the pitch of helix it decreased. The performance parameter, PEC= $((H_{2\,flux,\,helical}/H_{2\,flux,\,straight})/(\Delta P_{helical}/\Delta P_{straight}))$ is defined as the amount of H_2 permeation flux to pressure penalty of a tube to evaluate the overall performance of the helical tubes and have a better understanding of the effect of the coil diameter and helix pitch on H_2

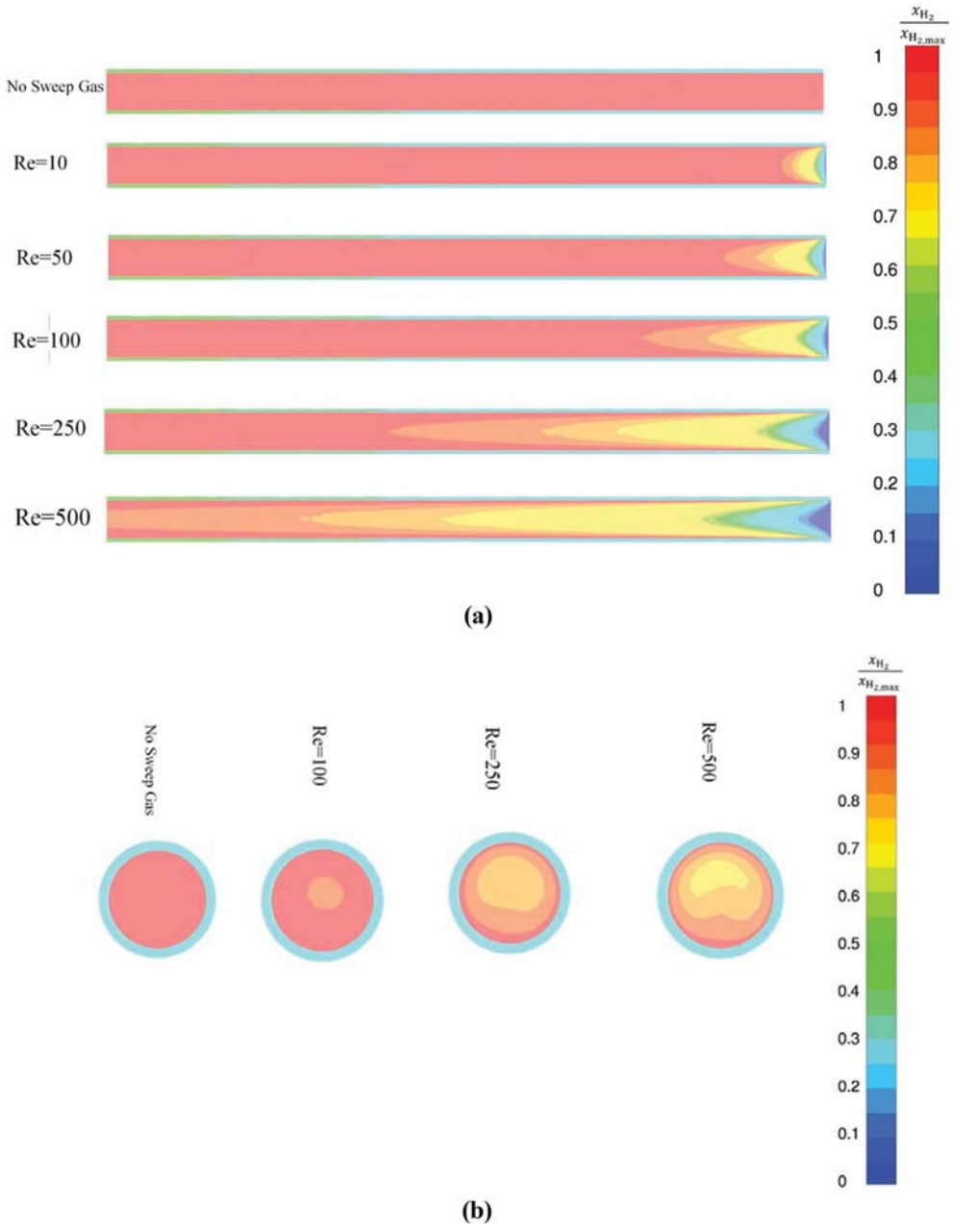

Fig. 14. H_2 concentration contours for different Reynolds numbers of sweep gas for the feed flow rate of 2,000 ml/min in (a) straight tube and (b) permeate side of a helical tube.

permeation and pressure drop, simultaneously. Fig. 13(b) shows the effect of using helical tubes. The higher values of *PEC* mean better performance, and to increase *PEC* the amount of H_2 permeation should be higher than the pressure drop. As can be seen, a helical tube with p=15 mm, d=10 mm, has the highest *PEC*. Note that although the larger coil diameter leads to a higher H_2 permeation, the higher pressure drop penalty of these tubes affects the overall performance and thus results in lower *PEC*.

2. Concentration Contours of H_2

To develop a better understanding of sweep gas flow rate effects on H_2 permeation, the concentration contours of H_2 in the straight and helical membrane tube for counter-current flow of sweep gas are demonstrated in Fig. 14. It is clearly seen that as the Reynolds number of the sweep gas increases, the molar fraction of hydrogen in the permeation side decreases, and it means that concentration polarization decreases radially. Hence, more hydrogen permeates through the membrane due to the increasing concentration gradient across the membrane. Consequently, the molar fraction of hydrogen in the retentate side is reduced; thus, the percentage of hydrogen recovery in the retentate increases.

3. Effect of Temperature

According to Sievert's law in membranes with a dominant mechanism of solution diffusion, the function of the membrane is ascending function of the temperature:

$$J_{sievert} = Q_0 \exp\left(-\frac{E_a}{RT}\right)(dP_i)^n \quad (6)$$

Therefore, it is expected that the profile of H_2 permeation flow is to be an ascending function of temperature as depicted in Fig. 15(a) and Fig. 15(b) for sweep gas of Re=100 and feed flow of 1,250 ml/min. However the figures do not precisely show the exponential behavior of temperature in Eq. (6), because with increasing temperature and thus increasing the membrane performance, other parameters, including the hydrogen recovery, also change and affect the overall performance of the membrane. Also, temperature change has changes the properties of gases, including the permeability of the mixture, viscosity, and density of the gas, which affects the membrane's function.

4. Effect of Pressure Difference on the Sides of the Membrane

Fig. 16(a) and Fig. 16(b), respectively, show the H_2 permeation and recovery as a function of a pressure difference between the feed and permeate flows for a sweep gas with Re=100 and feed flow of 1,250 ml/min. It is observed that increasing the pressure difference increases the partial pressure of the H_2 and thus increases the

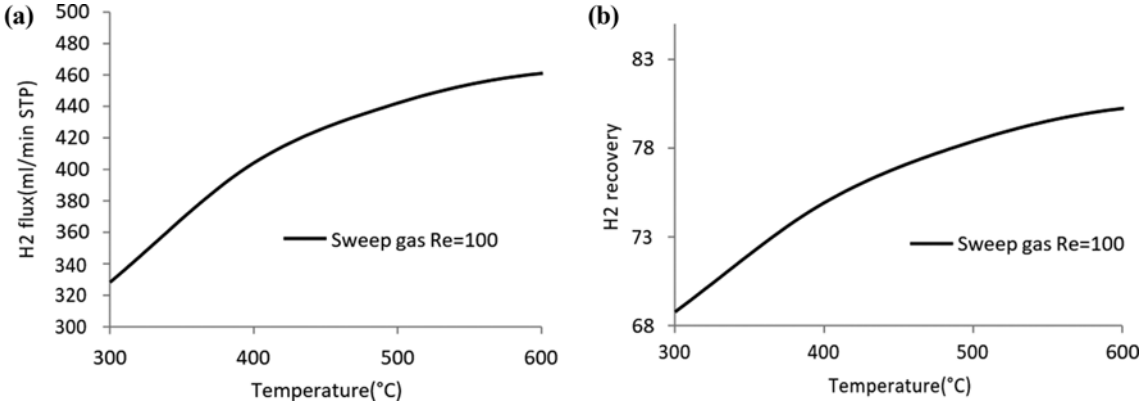

Fig. 15. Distribution of (a) H_2 Flow rate at the outlet of the permeate domain and (b) H_2 recovery in a straight tube for different temperatures.

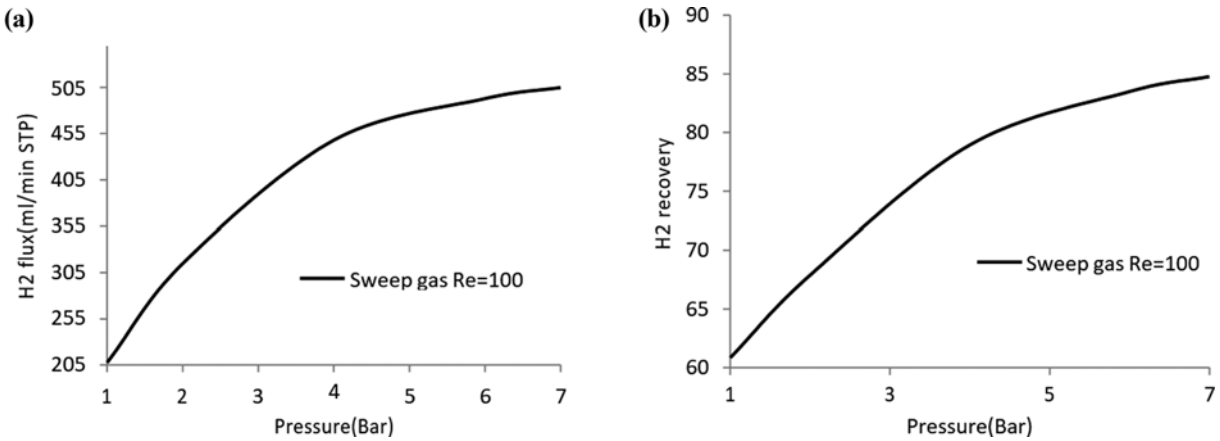

Fig. 16. Distribution of (a) H_2 Flow rate at the outlet of the permeate domain and (b) H_2 recovery in a straight tube for different amounts of pressure difference.

driving force, which leads to H_2 permeation and H_2 recovery enhancement. However, the rate of increase in H_2 permeation is decreasing, by increasing the total pressure difference, and the amount of H_2 permeation increases gradually.

CONCLUSIONS

A novel three-dimensional numerical model was developed to analyze the hydrogen separation of an H_2-N_2 gas mixture across a dense Pd membrane tube for straight and helical geometries. Unlike other methods in this method, H_2 permeation through a membrane is treated similarly to heat conduction equations without introducing a source-sink pair in the governing equations. The effects of feed gas flow rate and sweep gas Reynolds number on the performance of H_2 permeation in the straight and helical modules were studied. The numerical results indicate that the helical module has a better performance for H_2 separation and H_2 recovery due to the higher value of surface to volume ratio and the existence of secondary flows. For both geometries increasing the feed gas flow rate led to increasing H_2 separation and decreasing H_2 recovery. It is shown that for a specific value of feed gas flow rate, increasing the sweep gas flow rate increases the H_2 permeation, by removing H_2 on the permeate side adjacent to the membrane and increasing the gradient of the partial concentration of H_2 across the membrane in both helical and straight modules. By investigating the two significant parameters in helical modules, it was also shown that the helix pitch changes have a better performance on increasing the average amount of H_2 permeation flux than coil diameter. Although the larger coil diameter leads to a higher H_2 permeation, the higher pressure drop penalty of these tubes affects the overall performance and thus results in lower *PEC*. The results also suggest that increasing the temperature of the system and pressure difference on the sides of the membrane, intensifies the H_2 permeation and H_2 recovery.

NOMENCLATURE

A : area [m^2]
C : concentration [mol m^{-3}]
D : diffusion coefficient [$m^2 s^{-1}$]
E_a : activation energy [kJ mol^{-1}]
h_{conv} : convection coefficient [w $m^{-2}K^{-1}$]
h_{mass} : mass transfer coefficient [m s^{-1}]
J : mass diffusion flux [mol $m^{-2}s^{-1}$]
K : conductivity [w $m^{-1}K^{-1}$]
M : molar mass [g mol^{-1}]
n : exponent indicating pressure dependence
p_i : species *i* pressure [bar]
Q_0 : pre exponential factor [mol $m^{-2}s^{-1}pa^{-n}$]
$\dot{Q}$: heat power [w]
R : universal gas constant [J $mol^{-1}K^{-1}$]
T : temperature [K]
V : velocity [m s^{-1}]
x : molar fraction

Greek Symbols

Δ : difference
∇ : gradient
δ : thickness [m]
μ : viscosity [pa s]
ρ : density [kg m^{-3}]

Subscript

i : species *i*
∞ : fluid
s : surface
mix : mixture

REFERENCES

1. D.-H. Lee and D.-J. Lee, *Int. J. Hydrogen Energy*, **33**, 1618 (2008).
2. M. A. Rosen, *J. Power Energy Eng.*, **3**, 373 (2015).
3. C. J. Winter, *Int. J. Hydrogen Energy*, **34**, 3 (2009).
4. R. B. Gupta, *Hydrogen fuel: production, transport, and storage*, CRC Press, Boca Raton, Florida (2008).
5. M. Momirlan and T. Veziroglu, *Renew. Sustain. Energy Rev.*, **6**, 179 (2002).
6. F. Farshchi Tabrizi, S. A. H. S. Mousavi and H. Atashi, *Energy Convers. Manag.*, **103**, 1077 (2015).
7. T. V. Choudhary, A. K. Santra, C. Sivadinarayana, B. K. Min, C.-W. Yi, K. Davis and D. W. Goodman, *Catal. Lett.*, **77**, 1 (2001).
8. R. Z. Sørensen, L. J. E. Nielsen, S. Jensen, O. Hansen, T. Johannessen, U. Quaade and C. H. Christensen, *Catal. Commun.*, **6**, 232 (2005).
9. T. V. Choudhary, C. Sivadinarayana and D. W. Goodman, *Catal. Lett.*, **72**, 201 (2001).
10. A. Murugan and A. S. Brown, *Int. J. Hydrogen Energy*, **40**, 4233 (2015).
11. M. Sjardin, K. J. Damen and A. P. C. Faaij, *Energy*, **31**, 2555 (2006).
12. S. Peramanu, B. G. Cox and B. B. Pruden, *Int. J. Hydrogen Energy*, **24**, 424 (1999).
13. W. H. Chen, W. Z. Syu, C. I. Hung, Y. L. Lin and C. C. Yang, *Int. J. Hydrogen Energy*, **37**, 12679 (2012).
14. S. Barison, S. Fasolin, S. Boldrini, A. Ferrario, M. Romano, F. Montagner, S. M. Deambrosis, M. Fabrizio and L. Armelao, *Int. J. Hydrogen Energy*, **43**, 7989 (2018).
15. N. A. Al-Mufachi, N. V. Rees and R. Steinberger-Wilkens, *Renew. Sustain. Energy Rev.*, **47**, 551 (2015).
16. M. R. Rahimpour, F. Samimi, A. Babapoor, T. Tohidian and S. Mohebi, *Chem. Eng. Process. Intensif.*, **121**, 49 (2017).
17. R. J. W. Voncken, I. Roghair and M. van Sint Annaland, *Chem. Eng. Sci.*, **205**, 318 (2019).
18. K. Ghasemzadeh, N. J. Harasi, A. Iulianelli and A. Basile, *Int. J. Hydrogen Energy*, **45**, 7354 (2019).
19. X. Yang, S. Wang, B. Hu, K. Zhang and Y. He, *J. Membr. Sci.*, **581**, 269 (2019).
20. S. D. Vlaev, D. Dzhonova-Atanasova and I. Tsibranska, *Chem. Eng. Process. Intensif.*, **147**, 107738 (2020).
21. F. Xie, J. Liu, J. Wang and W. Chen, *Korean J. Chem. Eng.*, **33**, 2178 (2016).
22. B. Haddadi, C. Jordan, M. Miltner and M. Harasek, *J. Membr. Sci.*, **563**, 209 (2018).
23. K. Ghasemzadeh, R. Zeynali, F. Bahadori and A. Basile, *Int. J.*

Hydrogen Energy, **43**, 7683 (2018).
24. J. Marriott and E. Sørensen, *Chem. Eng. Sci.*, **58**, 4990 (2003).
25. X. Li, Y. Liu, H. Jiang and R. Chen, *Ind. Eng. Chem. Res.*, **58**, 1094 (2018).
26. S. A. Miramini, S. M. R. Razavi, M. Ghadiri, S. Z. Mahdavi and S. Moradi, *Chem. Eng. Process. Intensif.*, **72**, 136 (2013).
27. D.-Y. Shin, K.-R. Hwang, J.-S. Park and M.-J. Park, *Korean J. Chem. Eng.*, **32**, 1421 (2015).
28. G. Ji, G. Wang, K. Hooman, S. Bhatia and J. C. D. da Costa, *Chem. Sci. Eng.*, **6**, 12 (2012).
29. S.-E. Wu, Y.-C. Lin, K.-J. Hwang, T.-W. Cheng and K.-L. Tung, *Chem. Eng. Process. Intensif.*, **125**, 96 (2018).
30. G. Lee, K.-R. Hwang, J.-S. Park and M.-J. Park, *Korean J. Chem. Eng.*, **34**, 2373 (2017).
31. H. Takaba and S. I. J. Nakao, *J. Membr. Sci.*, **249**, 88 (2005).
32. M. M. Abdel-Jawad, S. Gopalakrishnan, M. C. Duke, M. N. Macrossan, P. Smith Schneider and J. C. Diniz da Costa, *J. Membr. Sci.*, **299**, 235 (2007).
33. M. Coroneo, G. Montante, M. Giacinti Baschetti and A. Paglianti, *Chem. Eng. Sci.*, **64**, 1094 (2009).
34. W. H. Chen, W. Z. Syu, C. I. Hung, Y. L. Lin and C. C. Yang, *Int. J. Hydrogen Energy*, **38**, 1156 (2013).
35. R. Ben-Mansour, H. Li and M. A. Habib, *Energy*, **144**, 626 (2018).
36. F. M. Ghohe and F. Hormozi, *Int. J. Hydrogen Energy*, **44**, 10665 (2019).
37. Y. A. Cengel and A. J. Ghajar, *Heat and mass transfer*, McGraw-Hill Educ., New York (2011).
38. S. C. Kluiters, *Energy Cent. Netherlands*, Petten, Netherlands (2004).
39. T. L. Ward and T. Dao, *J. Membr. Sci.*, **153**, 231 (1999).
40. W. P. Wang, S. Thomas, X. L. Zhang, X. L. Pan, W. S. Yang and G. X. Xiong, *Sep. Purif. Technol.*, **52**, 185 (2006).